Collision rate coefficient for charged dust grains in the presence of linear shear

Huan Yang and Christopher J. Hogan, Jr.

Phys. Rev. E **96**, 032911 — Published 18 September 2017

DOI: 10.1103/PhysRevE.96.032911

The Collision Rate Coefficient for Charged Dust Grains in the Presence of Linear Shear

Huan Yang & Christopher J. Hogan Jr.*

Department of Mechanical Engineering, University of Minnesota, 111 Church St. S.E., Minneapolis, MN, 55455, USA

Submitted To:

Physical Review E

***To whom correspondence should to be addressed: hogan108@.umn.edu, T: 612-626-8312**

ABSTRACT

Like and oppositely charged particles/dust grains in linear shear flows are often driven to collide with one another by fluid and/or electrostatic forces, which can strongly influence particle size distribution evolution. In gaseous media, collisions in shear are further complicated because particle inertia can influence differential motion. Expressions for the collision rate coefficient have not been developed previously which simultaneously account for the influences of linear shear, particle inertia, and electrostatic interactions. Here, we determine the collision rate coefficient accounting for the aforementioned effects by determining the collision area, i.e. the area of the plane perpendicular to the shear flow defining the relative initial locations of particles which will collide with one another. Integration of the particle flux over this area yields the collision rate. Collision rate calculations are parametrized as an enhancement factor, i.e. the ratio of the collision rate considering potential interactions and inertia to the traditional collision rate considering laminar shear only. For particles of constant surface charge density, the enhancement factor is found dependent only on the Stokes number (quantifying particle inertia), the electrostatic energy to shear energy ratio, and the ratio of colliding particle radii. Enhancement factors are determined for Stokes numbers in the 0-10 range and energy ratios up to 5. Calculations show that the influences of both electrostatic interactions and inertia are significant; for inertialess (St = 0) equal-sized and oppositely charged particles, we find that even at energy ratios as low as 0.2, enhancement factors are in excess of 2. For the same situation but liked-charged particles, enhancement factors fall below 0.5. Increasing the Stokes number acts to mitigate the influence of electrostatic potentials for both like and oppositely charged particles, i.e. inertia reduces the enhancement factor for oppositely charged particles and increases it for like charged particles. Uniquely, at elevated Stokes numbers with attractive potentials we find collisionless "pockets" within the collision area, which are regions completely bounded by the collision area but within which collisions do not occur. Regression equations to results are provided, enabling calculation of the enhancement factor as a function of energy ratio and Stokes number. In total, this study both leads to insight into the collision dynamics of finite-inertia, charged particles in shear flows, and provides a means to simply calculate the particle-particle collision rate coefficient.

\

I. INTRODUCTION

Collisions between micrometer sized charged particles/dust grains have a large influence on the behavior of many colloidal [1], aerosol [2,3], granular [4-6], and dusty plasma [7-9] systems. For example, in fluidized beds, dust storms, and volcanic plumes, particle-particle collisions lead to charge exchange (even for identical chemical composition particles [4,10-12]), which can significantly alter the behavior of a particle-laden flow [13-15]. In aerosols and dusty plasmas, oppositely charged particles rapidly aggregate (collide and bind) with one another, while the charging of particles to sufficiently high levels of the same polarity stabilizes them against aggregation [16-20]. Given the importance of charged particle collisions in particle-laden flows, numerous efforts have been devoted to developing accurate collision rate models for charged particles [21-23]. Many of these efforts consider the combined influences of electrostatic potential interactions and thermal energy on particle motion, such that the number of collisions per unit volume per unit time (R_{ij}) between particles of type i (size, charge level) and type j can be calculated as:

$$R_{ij} = k_{ij} n_i n_j \tag{1}$$

where n_i and n_j are the number concentrations of particles of type i and type j, respectively, and k_{ij} is the collision rate coefficient. In particular, in liquid colloids, the approach of Fuchs [24] has been used to calculate collision rate coefficients considering Brownian motion (continuum regime thermal motion) and combined electrostatic and van der Waals potential interactions (i.e. DLVO interactions)[25]. In reduced pressure systems, the effects of thermal energy and electrostatic forces have been incorporated into orbital motion limited (OML) theory based collision rate coefficient predictions [26-28]. A variety of approaches have also been utilized to derive collision rate expressions between the colloidal (diffusive) and low pressure (ballistic) limits [29-33], both for particles with one another as well as particles with ions. In large part, the aforementioned collision rate expressions have shown good agreement with experimental measurements [34,35], thus their incorporation into population balance models of particle ensembles is commonplace [36].

However, for micrometer sized particles in flowing systems, the influence of thermal energy on particle motion is often negligible in comparison to the influence that laminar (linear) shear gradients have on particle differential motion. This differential motion can lead to an enhanced rate of collisions (so-called orthokinetic aggregation) between particles as compared to consideration of thermal energy alone [37]. In the absence of any electrostatic interactions, the collision rate coefficient for spherical particles of radii a_i and a_j in the presence of a linear shear gradient G was first derived by Smoluchowski [38], and is given as:

$$k_{ij} = \frac{4}{3} G\left(a_i + a_j\right)^3 \tag{2a}$$

A number of studies have examined the combined influence of DLVO-like potential interactions (wherein particles electrostatically repel one another but attract one another at close approach via van der Waals interactions) and laminar shear gradients on particle collisions; collision rate coefficients derived considering these two approaches apply specifically to particles in liquid colloids [39-41]. However, a collision rate expression considering the combined influences of laminar shear and electrostatic potential interactions (both attractive and repulsive), which can be applied to particles in gaseous media (including granular systems, aerosols, clouds, and dust storms) remains undeveloped, despite the fact that in many gas phase systems, both electrostatic interactions and shear play a role in governing particle-particle collisions. The specific issues which remain to be addressed in modeling collisions in such systems are two-fold. First, when following the derivation of equation (2a) but considering attractive electrostatic interactions, the collision area (defined subsequently) approaches infinity. This complicates calculation of the integral required to determine the collision rate coefficient. Second, unlike liquid colloidal suspensions, larger shear gradients can persist in gaseous systems, and as such the influence of particle inertia on motion in a combined electrostatic and shear field can be significant. Prior approaches to collision rate coefficient evaluation have neglected particle inertial influences.

The purpose of this work is to utilize a trajectory based calculation approach to find an expression for the particle-particle collision rate coefficient in the presence of a linear shear gradient and electrostatic potential interactions, while also accounting for finite particle inertia. The resulting calculations are parametrized as an enhancement factor, η_L, such that the collision rate coefficient can be calculated in a manner analogous to equation (2a):

$$k_{ij} = \frac{4}{3} G\left(a_i + a_j\right)^3 \eta_L \tag{2b}$$

The sections that follow provide details on the trajectory calculations employed as well as on incorporation of trajectory calculation results into enhancement factor calculations. Subsequently, calculation results are presented considering simple Coulomb potentials as well as fully resolved electrostatic interactions for conducting particles. We parameterize enhancement factors as functions of a dimensionless electrostatic to shear energy ratio, the Stokes number, and the particle size (radius) ratio. The resulting expressions are applicable for calculations of particle-particle collision rates in gases wherein both shear gradients and electrostatic effects influence particle motion, but with thermal motion negligible.

II. THEORETICAL AND NUMERICAL APPROACH

In section IIA we derive the non-dimensionalized equation of motion applicable to particles used in collision rate determination (considering simple Coulomb and full electrostatic potential interactions), and then in section IIB we discuss the numerical methods employed to carry out trajectory and enhancement factor calculations. Readers not concerned with the details of calculations can directly focus on the Results & Discussion section without significant loss of scope.

A. The motion of charged particle pairs in a laminar shear field

Collisions can be modeled by examining particle pairs (i.e. we consider one particle *i* and a second *j*). The equation of motion for each charged particle in a linear shear field of magnitude G is given by:

$$m\frac{d^2\vec{R}(t)}{dt^2} = f\left[\vec{u}\big(\vec{R}(t)\big) - \frac{d\vec{R}(t)}{dt}\right] + \vec{F}_e \tag{3}$$

where m is the particle mass, $\vec{R}$ its position, $\vec{u}$ is the fluid velocity field (i.e. $\vec{u}(x,y,z) = -Gy\hat{e}_z$, where $\hat{e}_z$ is the unit vector in the z-direction and x, y, z are coordinates of an arbitrary point in a linear shear field with a gradient in the y-direction), and $\vec{F}_e$ is the electrostatic force between particles. In writing equation (3), Stokes drag is assumed, hence the drag coefficient takes the form of $f = 6\pi\mu a$, where a is the particle radius and μ is the gas dynamic viscosity. We find this is a reasonable assumption for the particle velocities obtained in trajectory simulations here, even in situations where the Stokes number is high. We note however, that we have neglected the slip correction factor [42] in our drag formulation. The slip correction factor could be easily incorporated into the subsequently presented dimensionless ratios with minimal modification to results. We also neglect the influences of viscous interactions [43] between particles at close approach, as well as Saffman lift forces [44]. We anticipate both influences are small for submicrometer to supermicrometer particles in the gas phase.

The electrostatic force acting on each particle can be obtained by differentiating the induced electrostatic potential energy, W:

$$\vec{F}_e = -\frac{dW}{dr_{ij}}\hat{r} \tag{4}$$

where $\hat{r}$ is the unit vector pointing from the center of the opposite particle to the present particle and r_{ij} is the scalar distance between particle centers. We examine interactions between non-conducting and perfectly conducting particles in the dilute limit. Under these conditions, the influence of screening on potentials is negligible (i.e. there is an infinite screening length). At the same time, when particles are far from one another, though potential interactions between particles are not screened, the effects of electrostatic forces on particle motion are negligible when compared to the effects of shear. Further, multibody interactions need not be considered in the dilute limit, as the probability that a third particle is in the vicinity of two particles closely approaching one another is zero. For non-conducting particles which have not yet collided, a simple two-body Coulomb potential is hence assumed, such that the potential energy between can be expressed as:

$$W = \frac{q_i q_j}{4\pi\varepsilon_0 r_{ij}} \tag{5}$$

where q is the charge carried by each of particles and ε_0 is the vacuum permittivity. For perfectly conducting particles, we utilize the functional form [45]:

$$W = \frac{q_i^2 c_{jj} - 2q_i q_j c_{ij} + q_j^2 c_{ii}}{8\pi\varepsilon_0(c_{ii}c_{jj} - c_{ij}^2)} \tag{6a}$$

where c_{ii}, c_{jj} and c_{ij} are the coefficients of capacitance, which are expressed as [46]:

$$c_{ii} = a_i(1-\kappa^2)\sum_{m=0}^{\infty}\frac{\alpha^m}{1-\kappa^2\alpha^{2m}} \tag{6b}$$

$$c_{ij} = -\frac{a_i a_j}{r_{ij}}(1-\alpha^2)\sum_{m=0}^{\infty}\frac{\alpha^m}{1-\alpha^{2(1+m)}} \tag{6c}$$

The dimensionless parameters α and κ are given by:

$$\alpha = \frac{{r_{ij}}^2 - {a_i}^2 - {a_j}^2}{2a_i a_j} - \sqrt{\left(\frac{{r_{ij}}^2 - {a_i}^2 - {a_j}^2}{2a_i a_j}\right)^2 - 1} \tag{6d}$$

$$\kappa = \frac{a_i + \alpha a_j}{r_{ij}} \tag{6e}$$

c_{jj} can be obtained by replacing a_i with a_j, and vice-versa in the expression of c_{ii}.

We define $t^* = Gt$, $\vec{R}^* = \vec{R}/(a_i + a_j)$, $\vec{u}^* = -y^* \hat{e}_z$ (where y^* the y-coordinate also normalized by a_i+a_j), $W^* = 4\pi\varepsilon_0(a_i + a_j)W/q_i q_j$, ${r_{ij}}^* = r_{ij}/(a_i + a_j)$, and $c^* = c/(a_i + a_j)$. The dimensionless equations of motion for particles *i* and *j* can then be obtained by combining equations (3-5) (for non-conducting particles), or equation (3) and equations (6a – 6c) (for conducting particles). For non-conducting particles the dimensionless equations are:

$$\frac{d^2 {\vec{R}_i}^*}{dt^{*2}} = (1 - \theta_\mathrm{m}) \frac{\mathrm{Q}}{\mathrm{St}} \frac{{\vec{R}_j}^* - {\vec{R}_i}^*}{{r_{ij}}^{*3}} - \frac{1 - \theta_\mathrm{m}}{(1 - \theta_\mathrm{f})\mathrm{St}} \left(\frac{d{\vec{R}_i}^*}{dt^*} - \vec{u}^* \left({\vec{R}_i}^*\right) \right) \tag{7a}$$

$$\frac{d^2 {\vec{R}_j}^*}{dt^{*2}} = \theta_\mathrm{m} \frac{\mathrm{Q}}{\mathrm{St}} \frac{{\vec{R}_i}^* - {\vec{R}_j}^*}{{r_{ij}}^{*3}} - \frac{\theta_\mathrm{m}}{\theta_\mathrm{f}\mathrm{St}} \left(\frac{d{\vec{R}_j}^*}{dt^*} - \vec{u}^* \left({\vec{R}_j}^*\right) \right) \tag{7b}$$

For conducting particles the dimensionless equations are:

$$\frac{d^2 {\vec{R}_i}^*}{dt^{*2}} = (1 - \theta_\mathrm{m}) \frac{\mathrm{Q}}{\mathrm{St}} \frac{{\vec{R}_i}^* - {\vec{R}_j}^*}{{r_{ij}}^*} \frac{dW^*}{d{r_{ij}}^*} - \frac{1 - \theta_\mathrm{m}}{(1 - \theta_\mathrm{f})\mathrm{St}} \left(\frac{d{\vec{R}_i}^*}{dt^*} - \vec{u}^* \left({\vec{R}_i}^*\right) \right) \tag{8a}$$

$$\frac{d^2 {\vec{R}_j}^*}{dt^{*2}} = \theta_\mathrm{m} \frac{\mathrm{Q}}{\mathrm{St}} \frac{{\vec{R}_j}^* - {\vec{R}_i}^*}{{r_{ij}}^*} \frac{dW^*}{d{r_{ij}}^*} - \frac{\theta_\mathrm{m}}{\theta_\mathrm{f}\mathrm{St}} \left(\frac{d{\vec{R}_j}^*}{dt^*} - \vec{u}^* \left({\vec{R}_j}^*\right) \right) \tag{8b}$$

$\frac{\mathrm{dW}^*}{\mathrm{dr_{ij}}^*}$ can be evaluated through the dimensionless form of equations (6a – 6c):

$$W^* = \frac{\theta_\mathrm{q} c_{jj}^* - 2c_{ij}^* + 1/\theta_q c_{ii}^*}{2(c_{jj}^* c_{ii}^* - {c_{ij}^*}^2)} \tag{9a}$$

$$c_{ii}^* = \theta_\mathrm{r}(1 - \kappa^2) \sum_{m=0}^{\infty} \frac{\alpha^m}{1 - \kappa^2 \alpha^{2m}} \tag{9b}$$

$$c_{ij}^{*} = -\frac{\theta_r(1-\theta_r)}{r_{ij}^{*}}(1-\alpha^2)\sum_{m=0}^{\infty}\frac{\alpha^m}{1-\alpha^{2(1+m)}} \tag{9c}$$

with the definitions $\alpha = \frac{{r_{ij}^{*}}^{2}-1+2\theta_r(1-\theta_r)}{2\theta_r(1-\theta_r)} - \sqrt{\left(\frac{{r_{ij}^{*}}^{2}-1+2\theta_r(1-\theta_r)}{2\theta_r(1-\theta_r)}\right)^2 - 1}$; $\kappa = \frac{\theta_r+\alpha(1-\theta_r)}{r_{ij}^{*}}$; $\theta_q = \frac{q_i}{q_j}$ and $\theta_r = \frac{a_i}{a_i+a_j}$. In calculating dimensionless potentials with equations (9b) and (9c) the number of terms retained in series (m_t) is determined by calculating the value of the series $\sum_{m=m_t+1}^{\infty}\left(\frac{\alpha^m}{1-\kappa^2}\right)$ and the series $\sum_{m=m_t+1}^{\infty}\left(\frac{\alpha^m}{1-\alpha^2}\right)$, for equations (9b) and (9c), respectively. These series have sums which are straightforward to calculate and are the respective upper limits for the series terms in (9b) and (9c). m_t is selected such that the upper limits are smaller than 0.01.

The dimensionless equations of motion show that the system, and hence the enhancement factor, is governed by six parameters: Q, St, θ_m, θ_f, θ_r, and θ_q (though θ_q only comes into play for conducting particles). They are the ratio of potential to kinetic energy, Stokes number, particle mass ratio, drag coefficient ratio, size ratio, and charge ratio, respectively. Q, St, θ_m, θ_f are calculated with the equations:

$$Q = \frac{-q_i q_j}{4\pi\varepsilon_0 f_{ij} G (a_i+a_j)^3} \tag{10a}$$

$$St = \frac{m_{ij}G}{f_{ij}} \tag{10b}$$

$$\theta_m = \frac{m_i}{m_i+m_j} \tag{10c}$$

$$\theta_f = \frac{f_i}{f_i+f_j} \tag{10d}$$

wherein $m_{ij} = \frac{m_i m_j}{m_i+m_j}$ and $f_{ij} = \frac{f_i f_j}{f_i+f_j}$. Q takes on positive values for oppositely charged particles and negative values for like charged particles. To reduce the number of cases necessary to examine, we note that for equivalent density particles in the continuum regime, $\theta_m = \left(\frac{a_i^3}{a_i^3+a_j^3}\right) = \left(\frac{\theta_r^3}{1-3\theta_r+3\theta_r^2}\right)$ and $\theta_f = \theta_r$ [47]. Additionally, under the assumption that irrespective of polarity, particles have similar surface charge densities, $\theta_q = \frac{\theta_r^2}{-1+2\theta_r-\theta_r^2}$ for oppositely charged particles and $\theta_q = \frac{\theta_r^2}{1-2\theta_r+\theta_r^2}$ for like-charged particles. This reduces the number of cases to examine, as now the enhancement factor is a function of Q, St, and θ_r only.

B. Enhancement factor calculation

We use trajectory calculations to determine the collision rate/enhancement factor for selected Q, St, and θ_r. In calculations, initially, particle *j* is placed at the origin of the coordinate system, with dimensionless Cartesian coordinates x^*,y^*, and z^* (each normalized by a_i+a_j). Particle *i* is released from a surface which is perpendicular to the direction of the shear flow, and is infinitely (100 dimensionless units in simulations) far from particle *j* (with an initial velocity of magnitude y^*, the dimensionless y coordinate). As noted in the prior section under such conditions particle velocities are defined only by the shear field; the potential is negligible initially. For each condition examined the equations of motion solutions are obtained via the Euler method with a fixed maximum distance traveled by each particle during a timestep (0.01 dimensionless units). A collision is considered to occur when the dimensionless center-to-center distance is less than 1.0. As demonstrated in the "Calculation validation and relative trajectories" section subsequently, we find this simple numerical algorithm is sufficient for accurate collision rate coefficient/enhancement factor determination under all circumstances. Sample trajectories are depicted in figure 1a, which specifically displays two views of particle *i* and particle *j* trajectories for two different initial release positions of particle *i*. For both sets of trajectories, attractive potential interactions between particles are considered, but there are different Q and St values, leading to a collision (upper images, with particles partially orbiting one another prior to collision) and non-collision (lower images), respectively.

For each input Q, St, and θ_r, a dimensionless collision area (S_c^*), can be obtained by recording the initial positions of particle *i* which lead to collision. With this dimensionless collision area, the dimensional collision rate would be expressed as:

$$k_{ij} = \left(a_i + a_j\right)^2 \iint_{S_c^*} v dS^* = \left(a_i + a_j\right)^3 G \iint_{S_c^*} y^* dS^* \tag{11}$$

where *v* denotes the initial relative speed between particles, which, in the case of linear shear, is equivalent to $(a_i+a_j)Gy^*$. In the absence of potentials, particles take straight line trajectories, and collisions only occur when the particles' initial center to center distance is less than or equal to the sum of their radii. S_c^* is hence a circular area of dimensionless radius of 1.0 with its center at the origin of the polar coordinate system. Substituting $dS^* = \rho^* d\rho^* d\theta$ and $y^* = \rho^* \cos(\theta)$ into equation (11), where ρ^* and θ are the dimensionless polar coordinate radial position and angle, respectively, leads to equation (2a) in the absence of potential interactions.

Considering potentials, the dimensionless enhancement factor can then be obtained by combining equation (2b) and equation (11):

$$\eta_L = \frac{3 \iint_{S_c^*} y^* dS^*}{4} \tag{12}$$

We adopt slightly different approaches for enhancement factor calculations considering attractive and repulsive interactions. For attractive interactions, we utilize a polar coordinate system on the release plane for type *i* particles. The pole of the polar coordinate system is located at the center of the collision area, and the polar axis is parallel to the y axis. We define ρ_b^* as the dimensionless boundary of the collision area. In doing so, we assume that for $\rho^*(\theta) \leq \rho_b^*(\theta)$, collision can occur, and outside of it collision does not occur. Equation (12) is then expressed as:

$$\eta_{L,0} = 3\int_0^{\frac{\pi}{2}}\int_0^{\rho_b^*(\theta)} \rho^{*2} cos\,(\theta)\, d\rho^* d\theta \qquad \text{(attractive potentials)} \qquad (13)$$

where the subscript "*0*" denotes the "baseline" enhancement factor calculated with the aforementioned ρ_b^* assumption (collision occurs). For 30-50 specific θ values (variable for different input conditions), ρ_b^* is determined by monitoring particle trajectories releasing particle *i* at a dimensionless radius of 1.0 and then at successively larger radii; $\rho_b^*(\theta)$ corresponds to the largest radial location at which collision occurs. $\rho_b^*(\theta)$ is not bounded as θ approaches $\pi/2$ because the initial velocity difference between particle *i* and *j* goes to zero, and because of the long-range nature of the Coulomb potential. This complicates the calculation of the integral in equation (13). We hence divide the collision area into *N* individual areas with the angle occupied by the *n*th area ranging from θ_{n-1} to θ_n. The contribution to collisions for each individual area can be calculated as:

$$\gamma_n = \int_{\theta_{n-1}}^{\theta_n}\int_0^{\rho_b^{*n}(\theta)} \rho^{*2} cos\,(\theta)\, d\rho^* d\theta,\ n = 1,2,..,N-1 \qquad (14)$$

$$\gamma_N = \int_{\theta_{N-1}}^{\frac{\pi}{2}}\int_0^{\rho_b^{*N}(\theta)} \rho^{*2} cos\,(\theta)\, d\rho^* d\theta \qquad (15)$$

The baseline enhancement factor is expressed as:

$$\eta_{L,0} = 3(\textstyle\sum_{n=1}^{n=N} \gamma_n) \qquad (16a)$$

To evaluate equations (14) and (15), expressions for θ_n, $\rho_b^{*n}(\theta)$ and $\rho_b^{*N}(\theta)$ need to be specified. We let $\theta_n = \frac{\pi}{2}(1 - \frac{1}{8^n})$, though note that the choice of this expression is arbitrary, and adopt it simply because it rapidly approaches $\frac{\pi}{2}$ at large *n*. We also adopt a function of the form: $\rho_b^{*n}(\theta) = A_n(\frac{1}{\frac{\pi}{2}-\theta})^{B_n} + C_n$. The coefficients A_n, B_n, and C_n are determined from the results of trajectory calculations yielding $\rho_b^{*n}(\theta)$ on the interval $\theta_{n-1} \leq \theta \leq \theta_n$. A depiction of the dimensionless collision area formed on the y^*- x^* plane, with ρ^*, θ_n, $\rho_b^{*n}(\theta)$, and γ_n each labelled, is provided in figure 1b. A regression example result for determination of A_n, B_n, and C_n is provided in the supplemental information. $\rho_b^{*N}(\theta)$ is the boundary for the collision area which consumes the angle from θ_{N-1} to $\frac{\pi}{2}$, and approaches infinity as $\theta \to \frac{\pi}{2}$. Because we can only use finite simulation data to fit $\rho_b^{*N}(\theta)$, there is some uncertainty in $\rho_b^{*N}(\theta)$, which further leads to the uncertainty of γ_N. However, we remark that there is no uncertainty in determination of $\rho_b^{*n}(\theta)$ and γ_n for $n < N$. Furthermore, as N increases, the value of γ_N decreases. Therefore, to compute η_L in the presence of attractive potentials, we iteratively increase N until the inequality $\frac{\gamma_N}{\sum_{n=1}^{n=N-1}\gamma_n} < 0.01$ is satisfied, and then approximate $\eta_{L,0} = 3(\sum_{n=1}^{n=N-1}\gamma_n)$. Because the assumed functional form for θ_n converges quickly to $\frac{\pi}{2}$ and because the assumed form for $\rho_b^{*n}(\theta)$ captures trajectory calculation results well, $N \leq 5$ is employed in most instances.

For low St simulations, the assumption that collision occurs for all $\rho^*(\theta) \leq \rho_b^*(\theta)$ is found valid. However, at St = 5 and St = 10, the two largest Stokes numbers examined, "pockets" within the collision area are found. These are regions of initial positions for which $\rho^*(\theta) \leq \rho_b^*(\theta)$ and collision does not occur, but which are completely circumscribed by a region of initial positions for which collision does occur. Such cases require corrections to the enhancement factor; to determine the bounds of pockets we examined trajectories with particle *i* released from a structured square grid within the bounds of $\rho_b^*(\theta)$, with a grid spacing of 0.01 dimensionless units. From these calculations we extract $\rho_i^*(\theta)$ and $\rho_o^*(\theta)$, the inner and outer radii of the pocket at the angle θ, respectively, as well as θ_1 and θ_2, the minimum and maximum angles where the pocket exists . The enhancement factor is then calculated correcting for the pocket area:

$$\eta_L = \eta_{L,0} - 3\int_{\theta_1}^{\theta_2}\int_{\rho_i^*(\theta)}^{\rho_o^*(\theta)} \rho^{*2} cos\,(\theta) d\rho^* d\theta \qquad \text{(attractive potentials)} \qquad (16b)$$

For repulsive interactions, the collision area is bounded, and in converse to the collisionless pockets found for attractive potentials, collisions only occur for $\rho_i^*(\theta) \leq \rho^* \leq \rho_o^*(\theta)$. The integral in equation (12) can thus be evaluated directly by summing up values of $y^* dS^*$in the region where collision occurs; this region can be determined by releasing particle *i* from a structured squared grid (again with a grid spacing of 0.01 dimensionless units, and with particle *i* released on the grid nodes).

III. RESULTS AND DISCUSSION

A. Calculation validation and relative trajectories

As enhancement factor calculations require implementation of trajectory calculations and subsequent numerical integration, it is critical to validate the method by determining enhancement factors through alternative means. We compare simulation results to those calculated more directly considering infinite Stokes number (St →∞, which signifies the influence of drag is negligible) with both attractive and repulsive Coulomb potentials. Though this situation is highly unphysical, as in order for shear to have an influence on particle motion the drag force must be significant, neglecting drag enables determination of the collision area boundaries directly from the conservation of energy and angular momentum for the colliding particles. Derived in the supplemental information following the approach of Vasil'ev & Reiss [48] but incorporating linear shear in lieu of thermal motion, the enhancement factor for St →∞ considering attractive Coulomb potentials can be calculated as:

$$\eta_L|_{\mathrm{St}\to\infty} = 3\int_0^{\frac{\pi}{2}}\int_0^{\sqrt{\frac{1}{2}+\frac{1}{2}\sqrt{1+\frac{8Q}{\cos^2(\theta)\mathrm{St}}}}} \rho^{*2}\cos(\theta)\, d\rho^* d\theta \qquad \text{(attractive)} \qquad (17a)$$

For the repulsive Coulomb potential, the enhancement factor is expressed as:

$$\eta_L|_{\mathrm{St}\to\infty} = 3\int_{\sqrt{\frac{1-\sqrt{1+8[Q/\mathrm{St}]}}{2}}}^{\sqrt{\frac{1+\sqrt{1+8[Q/\mathrm{St}]}}{2}}} \int_0^{\sqrt{1+\frac{2[Q/\mathrm{St}]}{y^{*2}}-y^{*2}}} y^* dx^* dy^* \qquad \text{(repulsive)} \qquad (17b)$$

Equation (17b) applies for negative values of Q, and for sufficiently large Q it does not result in real numbers; in these instances $\eta_L|_{\mathrm{St}\to\infty} = 0$. The consequence of St→∞ is that in equations (7a) and (7b) the drag term (rightmost term) can be neglected, with which it is evident that trajectory calculation results, similar to equations (17a) and (17b), are dependent primarily on the parameter Q/St (which is the ratio of electrical energy to initial particle translational energy). Equations (17a) and (17b) calculations are plotted in comparison to trajectory calculation results in figures 2a and 2b, respectively. Across multiple orders of magnitude in Q/St, we find excellent agreement with another for both attractive and repulsive collisions; in most circumstances the two approaches agree to within 1% of one another, supporting the use of trajectory calculations for enhancement factor determination.

In total, we determined η_L for more than 400 distinct St, Q, and θ_r combinations, considering attractive and repulsive potentials, both with the Coulomb and conducting electrostatic potential functional forms. Tables S1-S4 in the supplemental information summarize calculation results for St = 0, 0.5, 1.0, 5.0, and 10; each presented η_L is the result of more than 100 trajectory calculations, up to 2000 trajectories for instances where potential influences are large. In subsequent sections we discuss the results of these calculations considering attractive and repulsive interactions, respectively. However, first we examine selected relative trajectories of particles in the presence of attractive collisions in figure 3a, considering complete electrostatic potential interactions. The boundary for collision, $(y_i^* - y_j^*)^2 + (z_i^* - z_j^*)^2 = 1$, is marked in the figure for each condition displayed. Particle motion at St = 0, the inertialess limit, is examined with simplified, first order equations of motion; these equations can easily be derived from equations (8a-8b). Elevated Stokes number relative trajectories result from direct implementation of equations (8a-8b). At St = 0 - 1, the displayed trajectories reveal that at smaller initial separation distances (smaller $y_i^* - y_j^*$ in figure 3), collision occurs, while above a critical value, there is no collision. Additionally evident is that particles may "overshoot" one another (i.e. $z_i^* - z_j^*$ becomes negative prior to collision) and many instances particle relative kinetic energy can approach zero at a relative location near $y_i^* - y_j^* = 0$, where there is little-to-no fluid driven differential motion. In such instances with attractive potentials, particles will be directed to collide-with one another; this evident first for one of the trajectories displayed at St = 1. At higher Stokes numbers (5 and 10), the overshoot and directed motion towards collision are even more pronounced, and in addition we find that particles can take orbiting-like trajectories, completing an entire revolution about one another. Experimentally, in the presence of differential settling (gravity) and electrostatic interactions, orbiting-like trajectories have been observed in the gas-phase [5]; simulations here suggest that similar trajectories can be driven by shear and electrostatic forces. Interestingly, we also find at elevated Stokes number instances where collision does not occur in a narrow initial separation distance region, with the precise bounds of this region dependent on θ. This is evidenced in figure 3b, which displays plots of all initial relative coordinates in trajectory calculations leading to collisions. The collisionless pockets are evident in figure 3b plots for St = 5 and St = 10. Such collisionless pockets, which necessitate the use of equation (16b) in enhancement factor calculations, only persist in instances where linear shear, inertia, and electrostatic interactions all have an influence on particle relative motion; they are not present for St = 0 (no inertia) conditions, St = ∞ (no shear gradient) conditions, and Q = 0 (no electrostatic interactions) conditions. Pockets are hence a unique feature of charged particle collision dynamics in gaseous media where particles can attain sufficiently high inertia.

B. Enhancement factor for attractive potentials

Though a simpler problem to examine, collisions in the inertialess limit (St = 0) are of interest for smaller particles, hence we examine this scenario first. Considering the Coulomb potential only and attractive potentials, the inertialess enhancement factor as Q→∞ can be analytically derived:

$$\eta_L|_{\mathrm{St}\to 0,\mathrm{Q}\to\infty} = 3\pi \mathrm{Q} \tag{18}$$

Equation (18) leads to a dimensional collision rate coefficient which agrees exactly with the diffusion limited collision rate coefficient [24] at high potential energy to thermal energy ratios; this is because in both the laminar shear case and in the diffusive limit, only electrostatic forces and drag influence particle motion at high potential energy. In figure 4, we plot η_L as a function of Q considering both Coulomb and conducting electrostatic potentials at variable particle size ratios (θ_r) for St = 0. Considering only the Coulomb potential, the particle size ratio is found to have a minimal influence on the enhancement factor; size influences are more pronounced for the complete electrostatic potential, with the largest enhancement factors observed for equal sized particles with the electrostatic potential. Also noteworthy is that even for small values Q (i.e. Q = 0.1) the enhancement factor takes on values greater than 1.5 for all examined conditions. In air at 300 K with a shear rate of 10 s^{-1}, Q = 0.1 corresponds to a modest surface charge density of 44 nC m^{-2}, hence calculations suggest that charged particle collisions in shear flows cannot be accurately modeled without considering the influence of the charge itself.

Plots analogous to figure 4 but for Stokes numbers in the 0.5-10 range are displayed in figure 5. Qualitatively, plots at elevated Stokes number are similar to the curves obtained for inertialess particles; $\eta_L \rightarrow 1$ as $Q \rightarrow 0$, the highest enhancement factors are obtained for equal sized particles subjected to full electrostatic potentials, and at larger Q, η_L scales linearly with Q. However, enhancement factors for all Q are reduced at elevated Stokes numbers, e.g. for Q = 0.21, η_L decreases from 2.26 to 1.89 and then to 1.24 as St increases from 0 to 0.5 and then to 10, for equal sized particles subject to the electrostatic potential. At larger Q, more pronounced St effects are evident, and η_L at Q = 1.56 evolves from 14.74 to 5.48 as St increases from 0 to 10. The decrease in η_L can be partially (but not entirely) attributed to the collision pockets formed at high Stokes number; for example at Q = 5.97, St = 10, and θ_r =0.2, we find $\eta_{L,0}$ = 21.0 while the pocket correction (equation 16b) is 2.2 (leading to η_L = 18.8). These results collectively show that coupled with the influence of charge is the influence of particle inertia, and that neither can be neglected outright in modeling charged particle collisions in gaseous shear flows.

The influence of potentials on the enhancement factor is not well described by an additivity approximation, i.e. $\eta_L \neq 1 + 3\pi Q$. To parameterize results we fit results for equal sized (and hence equal but opposite charge level) particles to the functional forms:

$$\eta_L = 1 + 3\pi Q b_3[b_1 + (1 - b_1)\exp\left(-\frac{b_2}{Q}\right)] \tag{19}$$

These functional forms match the large and small Q limiting functional forms by design. The values of b_1, b_2, and b_3 provided in tables 1 and 2 for the Coulomb and complete electrostatic potentials, respectively, are found to match calculations extremely well (to within 1% of calculation results in most circumstances).

C. Enhancement factor for repulsive potentials

In all circumstances where long-range, repulsive interactions between particles are present, there will be a value of Q (absolute) above which the enhancement factor is zero. Therefore, an analogous expression to equation (18) need not be developed for repulsive potentials. Figure 6 displays plots of the enhancement factor versus –Q for St = 0 – 10, considering both repulsive Coulombic and complete electrostatic potentials (with the latter a repulsive potential at large separation distances, and an attractive potential at close separation distances). For repulsive potentials, again the enhancement factor is higher for the complete electrostatic potential in comparison to the Coulomb potential, which is attributable to the close range attraction incorporated into this potential form. While for purely attractive interactions particle inertia leads to decreased enhancement factors with increasing St, for repulsive potentials, the enhancement factor increases with increasing St, and drastically so. For example at Q = -0.63, with St = 0, particle-particle collisions will not occur, irrespective of particle size ratio. Under the same conditions but with St = 10, the enhancement factor remains above 0.55 (for all potentials and size ratios), suggesting that though repulsive interactions decrease the rate of particle-particle collisions, it remains similar in magnitude to that for uncharged particles.

For equal sized particles, we fit repulsive potential results to the functional form:

$$\eta_L = c\mathrm{Q}^2 + (c\mathrm{Q}_0 + 1/\mathrm{Q}_0)\mathrm{Q} + 1, \quad |Q| < \mathrm{Q}_0; \;\; \eta_L = 0, \; |Q| \geq \mathrm{Q}_0 \qquad (20)$$

Regression values for c and Q_0 (the absolute value of Q above which collisions no longer occur) are provided in tables 3 and 4 for the Coulomb and complete electrostatic potentials, respectively.

D. Comparison to diffusion limited collision rates

An interesting comparison is the collision rate for oppositely charged particles in the presence of a laminar shear gradient to that predicted by the diffusion limited reaction theory [31,36,49], i.e. evaluation of whether Brownian motion or differential fluid motion has a greater influence on charged particle collisions. Consideration of inertialess, equal sized particles and the Coulomb potential enables direct derivation of $\frac{k_{ij}|_L}{k_{ij}|_B}$, the laminar shear to Brownian motion collision rate coefficient:

$$\frac{k_{ij}|_L}{k_{ij}|_B} = \left(1 - exp(-\Lambda Q)\right)\left(\frac{1}{3\pi Q} + \left(b_1 + (1 - b_1)exp\left(\frac{-b_2}{Q}\right)\right)\right) \tag{21}$$

where $\Lambda = \frac{Gf_{ij}\left(a_i + a_j\right)^2}{kT}$ is the shear energy to thermal energy ratio (kT is the thermal energy). Equation (21) is plotted in figure 7 for selected values of Λ. Immediately apparent is that only in instances of high Λ (larger than 3π) and modest values of Q (below 1) will the laminar shear collision rate exceed the Brownian motion collision rate. In converse to prior sections, which demonstrate the importance of considering both charge and inertial influences on particle-particle collisions in shear flows, figure 7 clearly shows that such phenomena need only be considered at high Λ. As Λ approximately scales with the cube of the particle radii (neglecting non-continuum drag effects), shear based collisions hence become significant above a critical size, determined by $\Lambda = 3\pi$. In air at 300 K, with G = 10 s^{-1}, the critical particle radius is 1.78 μm, while at G = 1 s^{-1}, the critical radius increases to 3.85 μm. Though density dependent, particles in this size range would still have Stokes numbers close to 0 (St < 0.001 for unit density particles under both example conditions); with shear gradients in the 10^0-10^2 s^{-1} range Stokes number influences on collisions manifest themselves for particles with radii in excess of 10 μm.

IV. CONCLUSIONS

We have developed and utilized a trajectory based approach to determine the enhancement factor for collisions between charged particles in a laminar/linear field in a gas, accounting for finite particle inertia. Electrical effects are parameterized by the electrical energy to shear energy ratio (Q), while inertial effects are parameterized by the Stokes number (St). With the enhancement factor, particle-particle collision rates can be calculated simply via equation (2b). We provide regression equations to better facilitate enhancement factor calculations for equal sized particles charged to equal levels. Based on our computations, we make the following concluding remarks:

1. In gaseous systems with appreciable shear gradients, the interplay between particle charge and particle inertia can strongly impact particle-particle collision rates. Use of simplified models of particle-particle collisions (i.e. equation (2a)) may lead to highly inaccurate predictions of collision rates, for both oppositely charged particles (where equation (2a) leads to underprediction) and particles of the same polarity (where it leads to overprediction). Particle inertia is found to lessen the influence of charge on collision, both for oppositely charged and like-charged particles, though not to the extent that charge effects can be ignored.
2. At moderate to large Stokes numbers (i.e. 5-10), we find collisionless pockets in the collision area for attractive potentials, which are regions of relative initial particle positions where collision does not occur, but which are completely circumscribed by

relative initial positions which lead to collision. To our knowledge such pockets have not been observed previously in examining particle-particle collision rates in liquid media or considering other forms of differential motion (i.e. settling), and appear to be a unique result of inertia, shear, and electrostatic interactions all influencing particle motion.

3. For charged particles (as well as uncharged particles, though not examined here), shear based motion need only be consider for modest Q levels and high shear energy to thermal energy ratios (above 3π). The shear energy to thermal energy ratio is strongly dependent on particle size, and is also influenced by gas viscosity, temperature, and through the friction coefficient, mean free path (if non-Continuum drag is considered). Above a critical size for any given system, shear induced motion is significantly more important than Brownian motion in driving particle-particle collisions. More refined analysis will be required to consider instances where shear induced motion, electrostatic interactions, inertia, and Brownian motion [50] all influence particle dynamics.
4. The collision rate described in this work refers to the rate of initial collisions between two particles in a dilute system; whether particles bind and aggregate, rebound and exchange charge, or recollide [5] has not been considered here. To investigate these phenomena in future work the approach employed here will need to be coupled with models of adhesion (i.e. more detailed short range potential interactions than the models employed here), charge exchange upon collision, and exchange of momentum and energy upon collision. Also not examined were aspherical particles and aggregates [23,51-53]; this will require consideration of alignment and rotation in

flow, as well as an appropriate drag coefficient [54]. Finally, many instances the dilute approximation is not valid, and multi-body particle interactions (particularly electrostatic) will need to be considered in future collision modeling efforts.

V. ACKNOWLEDGMENTS

H. Y. acknowledges support from the 3M Fellowship. Partial support was also provided by the United States Army Research Office Award MURI W911NF-12-0407.

VI. SUPPLEMENTAL INFORMATION

Tables S1-S4 summarizing calculation results, figure S1 and table S5, showing an example regression result used in collision area boundary determination, and derivation of equations (17a) and (17b) are available online.

VII. REFERENCES

[1] N. I. Lebovka, in *Polyelectrolyte Complexes in the Dispersed and Solid State I: Principles and Theory*, edited by M. Muller (Springer-Verlag Berlin, Berlin, 2014), pp. 57.

[2] A. A. Onischuk, S. di Stasio, V. V. Karasev, A. M. Baklanov, G. A. Makhov, A. L. Vlasenko, A. R. Sadykova, A. V. Shipovalov, and V. N. Panfilov, J. Aerosol. Sci. **34**, 383 (2003).

[3] S. Vemury and S. E. Pratsinis, J. Aerosol. Sci. **27**, 951 (1996).

[4] K. M. Forward, D. J. Lacks, and R. M. Sankaran, Physical Review Letters **102**, 028001 (2009).

[5] V. Lee, S. R. Waitukaitis, M. Z. Miskin, and H. M. Jaeger, Nat Phys **11**, 733 (2015).

[6] P. Mehrani, M. Murtomaa, and D. J. Lacks, Journal of Electrostatics **87**, 64 (2017).

[7] O. Ishihara, J. Phys. D-Appl. Phys. **40**, R121 (2007).

[8] G. E. Morfill and A. V. Ivlev, Reviews of Modern Physics **81**, 1353 (2009).

[9] L. C. J. Heijmans and S. Nijdam, EPL (Europhysics Letters) **114**, 64004 (2016).

[10] D. J. Lacks and R. M. Sankaran, J. Phys. D-Appl. Phys. **44**, 453001 (2011).

[11] T. Pahtz, H. J. Herrmann, and T. Shinbrot, Nat Phys **6**, 364 (2010).

[12] R. Yoshimatsu, N. A. M. Araújo, G. Wurm, H. J. Herrmann, and T. Shinbrot, Scientific Reports **7**, 39996 (2017).

[13] T. Shinbrot and H. J. Herrmann, Nature **451**, 773 (2008).

[14] M. F. Al-Adel, D. A. Saville, and S. Sundaresan, Industrial & Engineering Chemistry Research **41**, 6224 (2002).

[15] D. J. Lacks and R. M. Sankaran, Particulate Science and Technology **34**, 55 (2016).

[16] U. Kortshagen and U. Bhandarkar, Phys. Rev. E **60**, 887 (1999).

[17] R. Le Picard, A. H. Markosyan, D. H. Porter, S. L. Girshick, and M. J. Kushner, Plasma Chemistry and Plasma Processing **36**, 941 (2016).

[18] L. Ravi and S. L. Girshick, Phys. Rev. E **79**, 026408 (2009).

[19] T. Matsoukas and M. Russell, Journal of Applied Physics **77**, 4285 (1995).

[20] T. Matsoukas, M. Russell, and M. Smith, Journal of Vacuum Science & Technology A: Vacuum, Surfaces, and Films **14**, 624 (1996).

[21] W. H. Marlow, Journal of Chemical Physics **73**, 6284 (1980).

[22] D. D. Huang, J. H. Seinfeld, and K. Okuyama, Journal of Colloid and Interface Science **141**, 191 (1991).

[23] A. Shahravan, C. Lucas, and T. Matsoukas, Journal of Applied Physics **108**, 083303 (2010).

[24] N. A. Fuchs, *The mechanics of aerosols* (Macmillan, New York,, 1964), Rev. and enl. edn.

[25] R. Hogg, T. W. Healy, and D. W. Fuerstenau, Transactions of the Faraday Society **62**, 1638 (1966).

[26] H. M. Mott-Smith and I. Langmuir, Physical Review **28**, 727 (1926).

[27] J. E. Allen, Phys. Scr. **45**, 497 (1992).

[28] J. Goree, Plasma Sources Sci. Technol. **3**, 400 (1994).

[29] N. A. Fuchs, Geofis. Pura Appl. **51**, 185 (1963).

[30] W. A. Hoppel and G. M. Frick, Aerosol Science and Technology **5**, 1 (1986).

[31] R. Gopalakrishnan and C. J. Hogan, Phys. Rev. E **85**, 026410 (2012).

[32] R. Gopalakrishnan, T. Thajudeen, H. Ouyang, and C. J. Hogan, J. Aerosol. Sci. **64**, 60 (2013).
[33] A. A. Lushnikov and M. Kulmala, Phys. Rev. E **70**, 046413 (2004).
[34] J. Porstendorfer, G. Robig, and A. Ahmed, J. Aerosol. Sci. **10**, 21 (1979).
[35] M. Adachi, Y. Kousaka, and K. Okuyama, J. Aerosol. Sci. **16**, 109 (1985).
[36] T. Matsoukas, Journal of Colloid and Interface Science **187**, 474 (1997).
[37] L. G. B. Bremer, P. Walstra, and T. Vanvliet, Colloid Surf. A-Physicochem. Eng. Asp. **99**, 121 (1995).
[38] M. van Smoluchowski, Zeit. Phys. Chem **92**, 129 (1917).
[39] M. Vanni and G. Baldi, Advances in Colloid and Interface Science **97**, 151 (2002).
[40] D. N. Thomas, S. J. Judd, and N. Fawcett, Water Research **33**, 1579 (1999).
[41] K. Higashitani, R. Ogawa, G. Hosokawa, and Y. Matsuno, Journal of Chemical Engineering of Japan **15**, 299 (1982).
[42] M. D. Allen and O. G. Raabe, Aerosol Science and Technology **4**, 269 (1985).
[43] L. A. Spielman, Journal of Colloid and Interface Science **33**, 562 (1970).
[44] P. Saffman, Journal of fluid mechanics **22**, 385 (1965).
[45] J. Lekner, Proceedings of the Royal Society A: Mathematical, Physical and Engineering Science (2012).
[46] J. H. Jeans, *The mathematical theory of electricity and magnetism* (University Press, 1908).
[47] T. Thajudeen, R. Gopalakrishnan, and C. J. Hogan, Aerosol Science and Technology **46**, 1174 (2012).
[48] O. V. Vasil'ev and H. Reiss, The Journal of Chemical Physics **105**, 2946 (1996).
[49] L. G. D'yachkov, A. G. Khrapak, S. A. Khrapak, and G. E. Morfill, Physics of Plasmas **14**, 042102 (2007).
[50] Y. Drossinos and M. W. Reeks, Phys. Rev. E **71**, 031113 (2005).
[51] W. R. Heinson, C. M. Sorensen, and A. Chakrabarti, Langmuir **28**, 11337 (2012).
[52] C. M. Sorensen and A. Chakrabarti, Soft Matter **7**, 2284 (2011).
[53] L. Isella and Y. Drossinos, Physical Review E **82**, 011404 (2010).
[54] C. Zhang, T. Thajudeen, C. Larriba, T. E. Schwartzentruber, and C. J. Hogan, Aerosol Science and Technology **46**, 1065 (2012).

Table 1. Equation (19) regression parameters for equal sized particles considering the attractive Coulomb potential.

St	b_1	b_2	b_3
0	0.5104	0.2302	1.0000
0.01	0.5389	0.3103	1.0174
0.02	0.5364	0.2991	1.0074
0.05	0.5297	0.3070	0.9916
0.1	0.5321	0.3319	0.9638
0.2	0.5208	0.3170	0.8985
0.5	0.5253	0.3973	0.7672
1	0.5168	0.4734	0.6349
2	0.4689	0.5177	0.5141
5	0.2681	0.4106	0.4149
10	0.1584	0.4022	0.3805

Table 2. Equation (19) regression parameters for equal sized particles considering the attractive electrostatic potential.

St	b_1	b_2	b_3
0	0.9949	32.2759	1.0000
0.01	0.9790	5.0819	1.0160
0.02	0.9748	7.8983	1.0141
0.05	0.9909	2.5547	0.9743
0.1	0.8426	0.5888	0.9511
0.2	0.9671	2.0743	0.8931
0.5	0.9241	1.4361	0.763
1	0.8738	0.7967	0.6251
2	0.7882	0.5944	0.5072
5	0.6521	0.4555	0.3994
10	0.2601	0.0933	0.3132

Table 3. Equation (20) regression parameters for equal sized particles subjected to the repulsive Coulomb potential.

St	*c*	Q_0
0	4.745	0.4348
0.01	4.689	0.4389
0.02	4.679	0.4348
0.05	4.498	0.4348
0.1	4.249	0.4308
0.2	3.689	0.4308
0.5	2.111	0.4348
1	0.888	0.4836
2	0.331	0.6211
5	0.123	1.0445
10	0.062	1.7392

Table 4. Equation (20) regression parameters for equal sized particles subjected to the repulsive electrostatic potential.

St	*c*	Q_0
0	2.510	0.6322
0.01	2.471	0.6379
0.02	2.479	0.6321
0.05	2.431	0.6321
0.1	2.328	0.6321
0.2	2.130	0.6321
0.5	1.542	0.6332
1	0.759	0.6575
2	0.226	0.7820
5	0.078	1.2542
10	0.038	2.0282

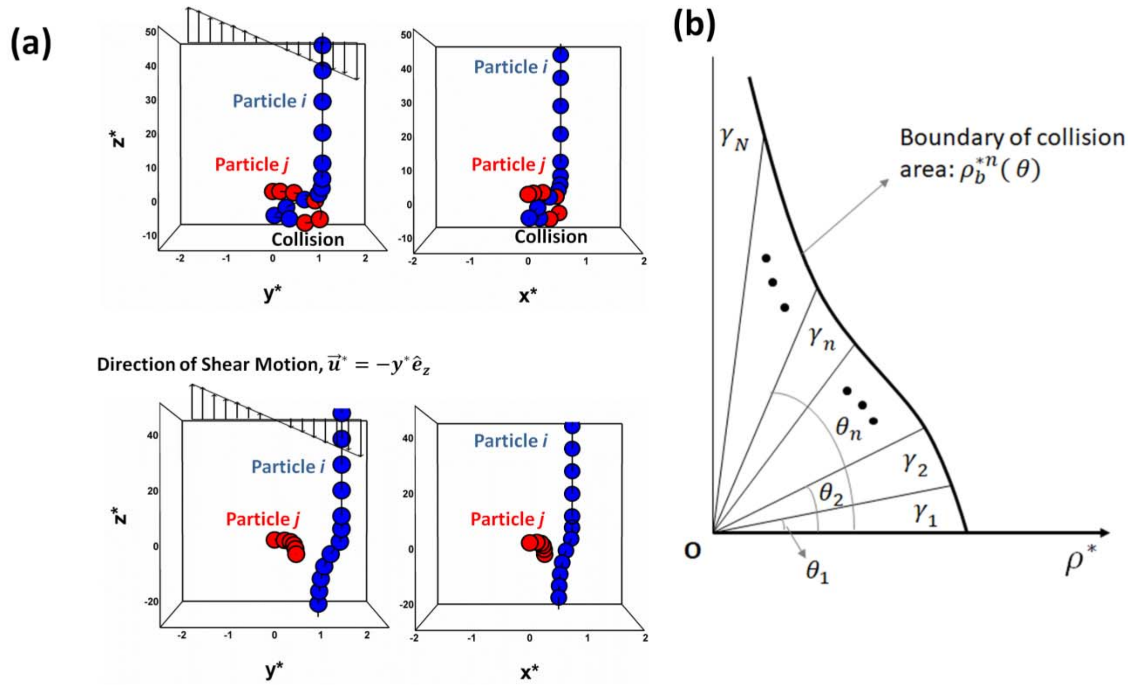

Figure 1. **(a)** Example results for trajectory calculations, wherein particle *j* is placed in the center of a linear shear field, and particle *i* is placed at a specific location at a large "z^*" distance from particle *j*. The trajectories displayed correspond to different Q and St values, as well as different initial positions, with the upper set corresponding to a collision, and the lower corresponding to a non-collision. Particle *j* only moves in response to the shear field after electrostatic forces brought about by the close approach of particle *i* move it from its original y^* position. **(b)** A depiction of the dimensionless collision area formed considering attractive potentials on the y^*-x^* plane.

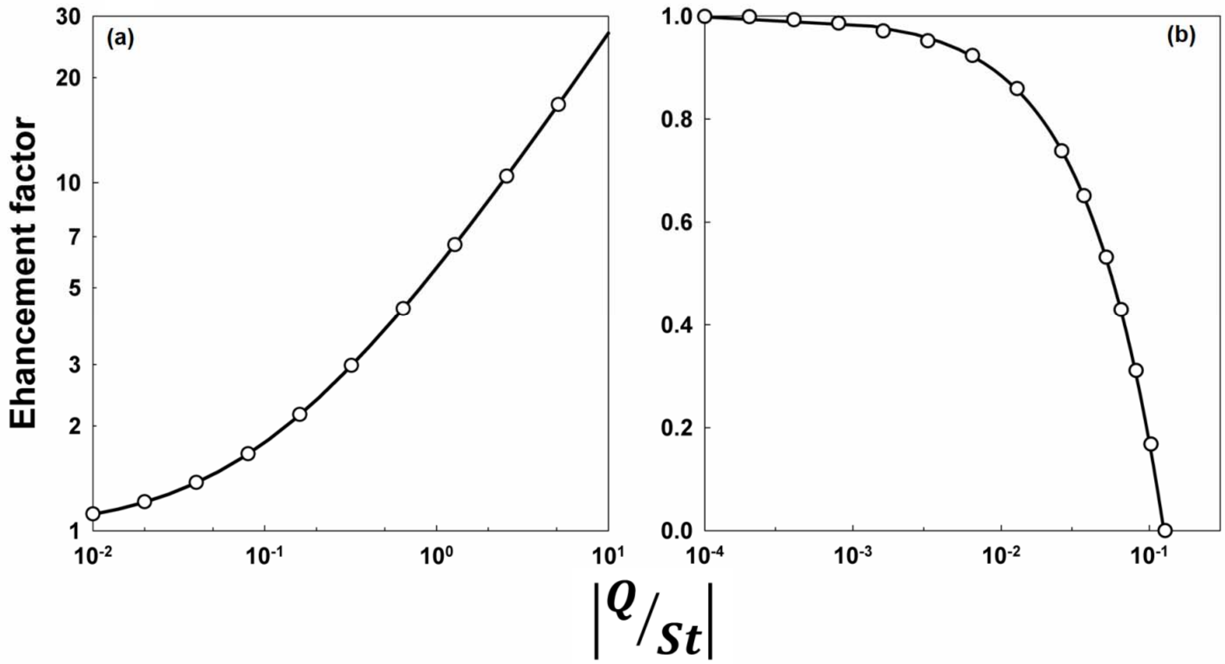

Figure 2. The calculated enhancement factor in the presence of laminar/linear shear considering (**a**) attractive and (**b**) repulsive Coulomb interactions between particles in the St→∞ limit. Open symbols: trajectory calculation results. Lines: equation (17a) and equation (17b) predictions.

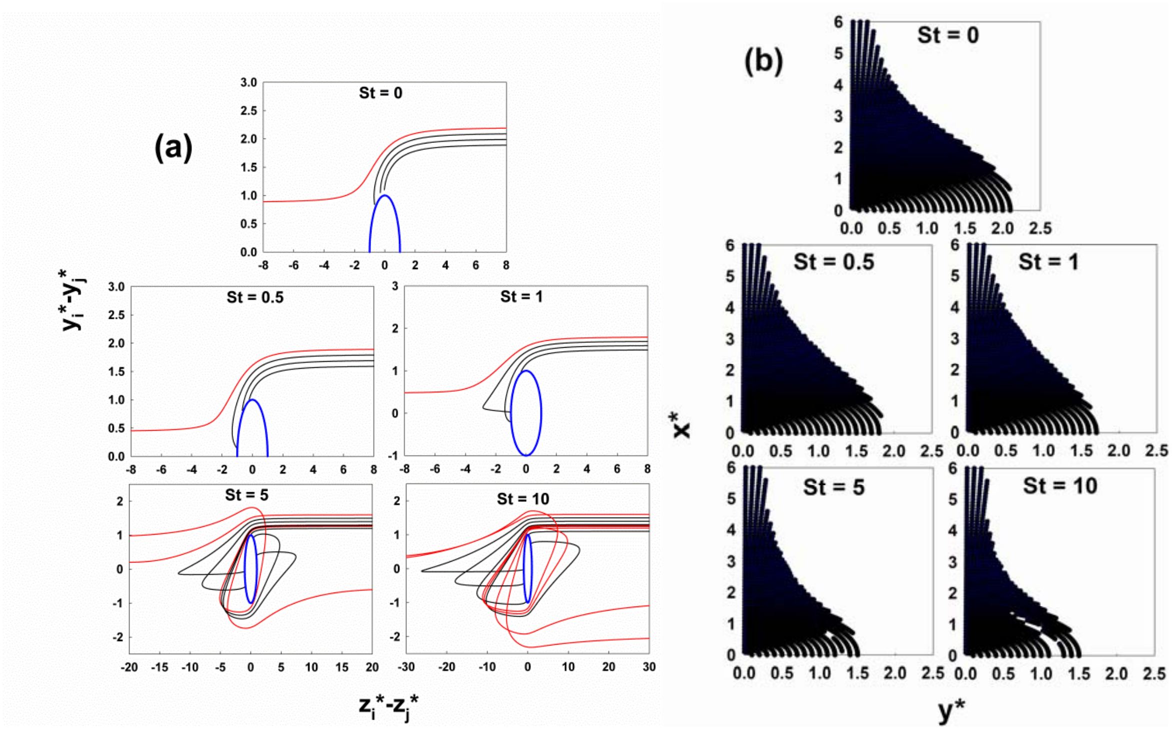

Figure 3. **(a)** Selected relative particle trajectories (i.e. the motion of particle *i* from the perspective of particle *j*) for particles initiated on the y^*, z^* ($x^* = 0$) plane. Black lines denote collision, while red lines denote non-colliding trajectories. The blue line denotes the bound $\left(y_i^* - y_j^*\right)^2 + \left(z_i^* - z_j^*\right)^2 = 1$, hence it is the collision boundary. **(b)** Points corresponding to initial relative release points leading to collision. Collisionless pockets are evident at St = 5 and St= 10. For all instances, Q = 1.56 and θ_r = 1.0, with the full electrostatic potential considered.

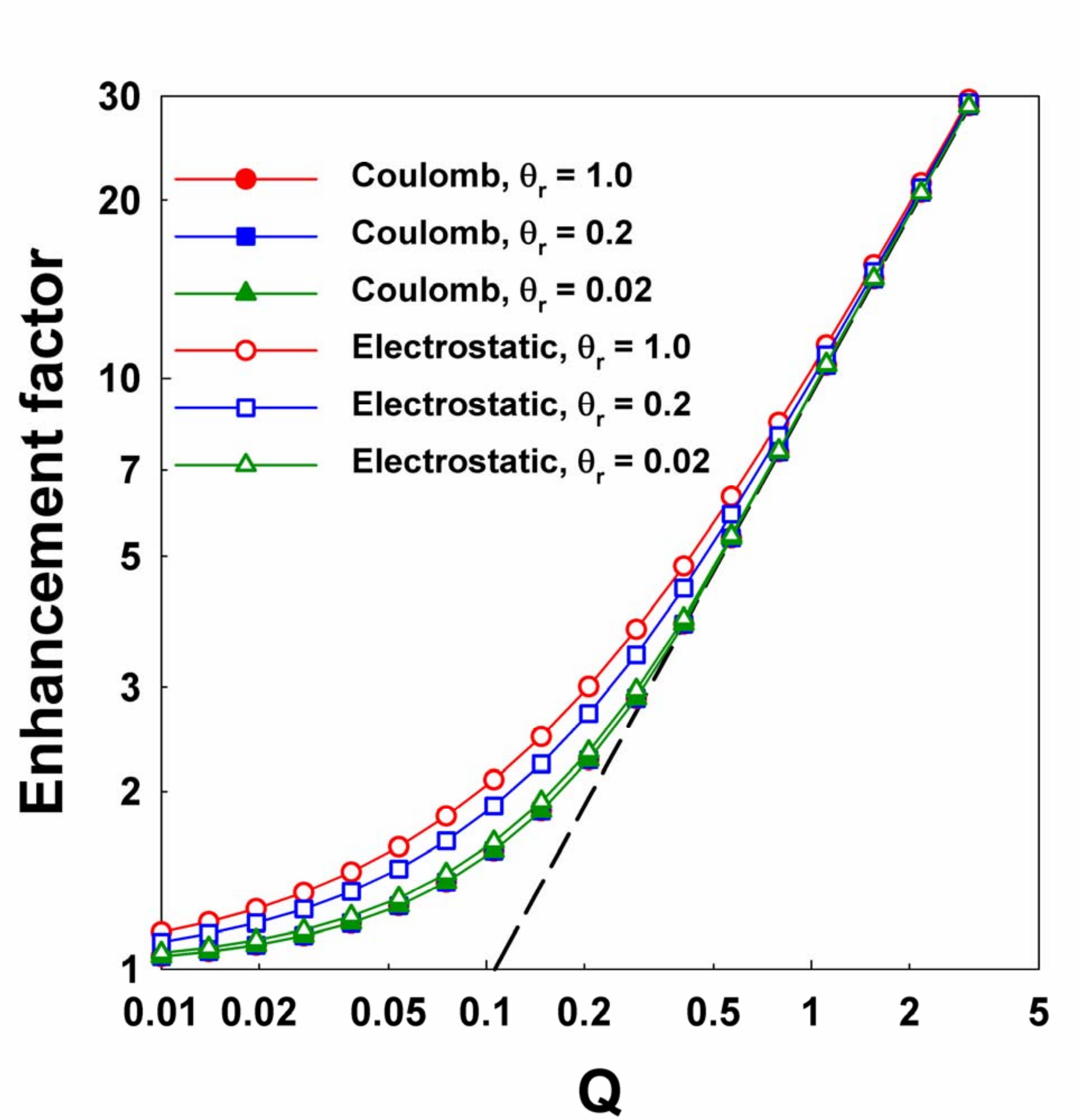

Figure 4. The enhancement factor considering attractive potential interactions for St = 0. The black dashed line denotes equation (18) predictions.

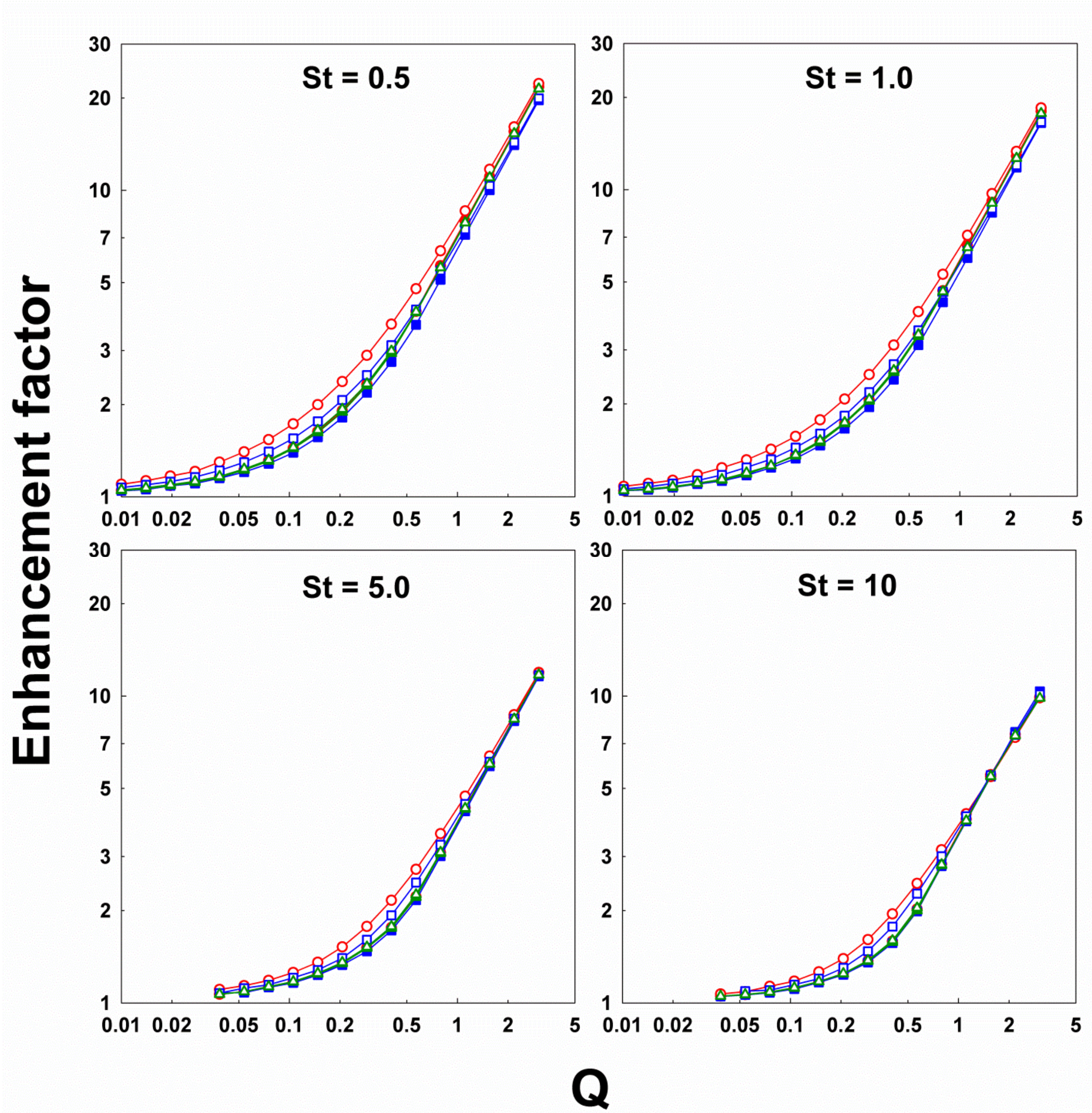

Figure 5. The enhancement factor considering attractive potential interactions for St = 0.5-10. The legend provided in Figure 4 applies to all displayed curves.

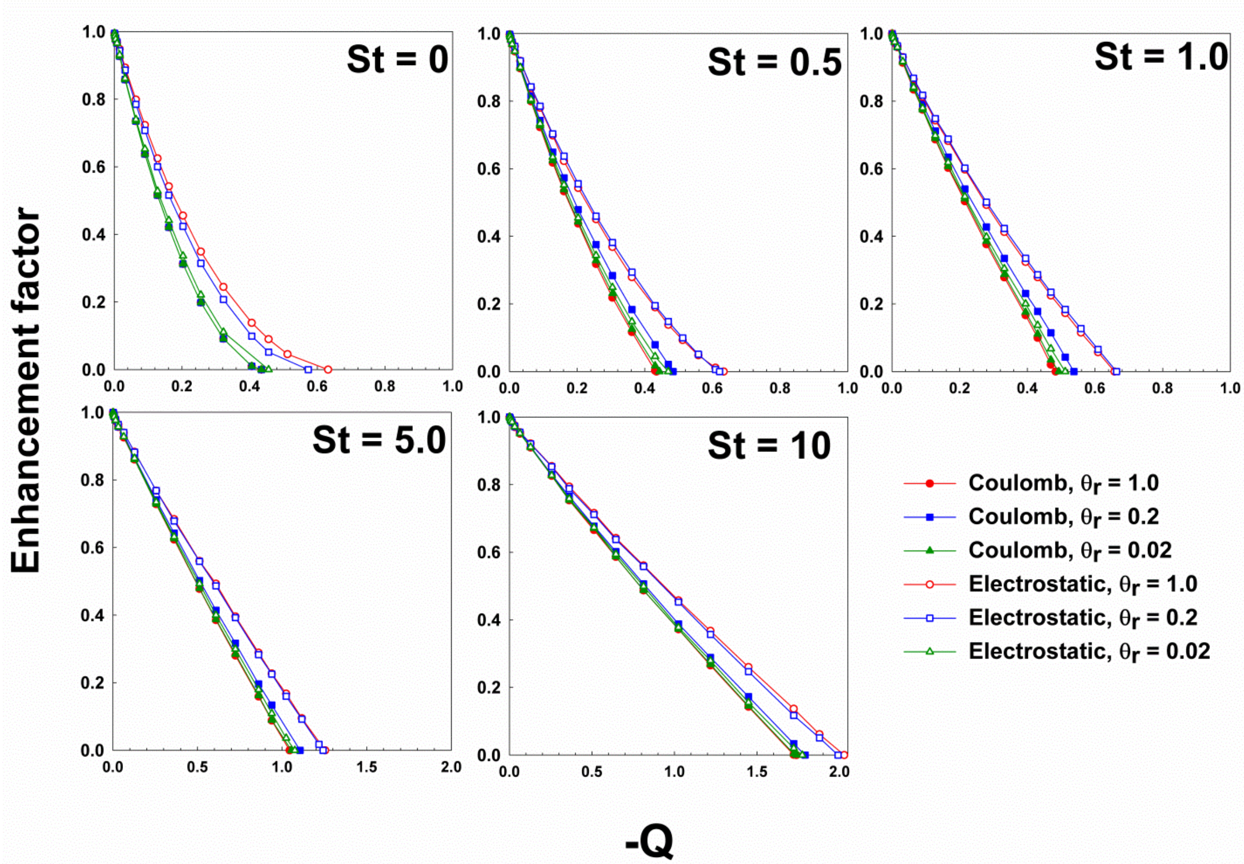

Figure 6. The enhancement factor as a function of –Q for repulsive interactions.

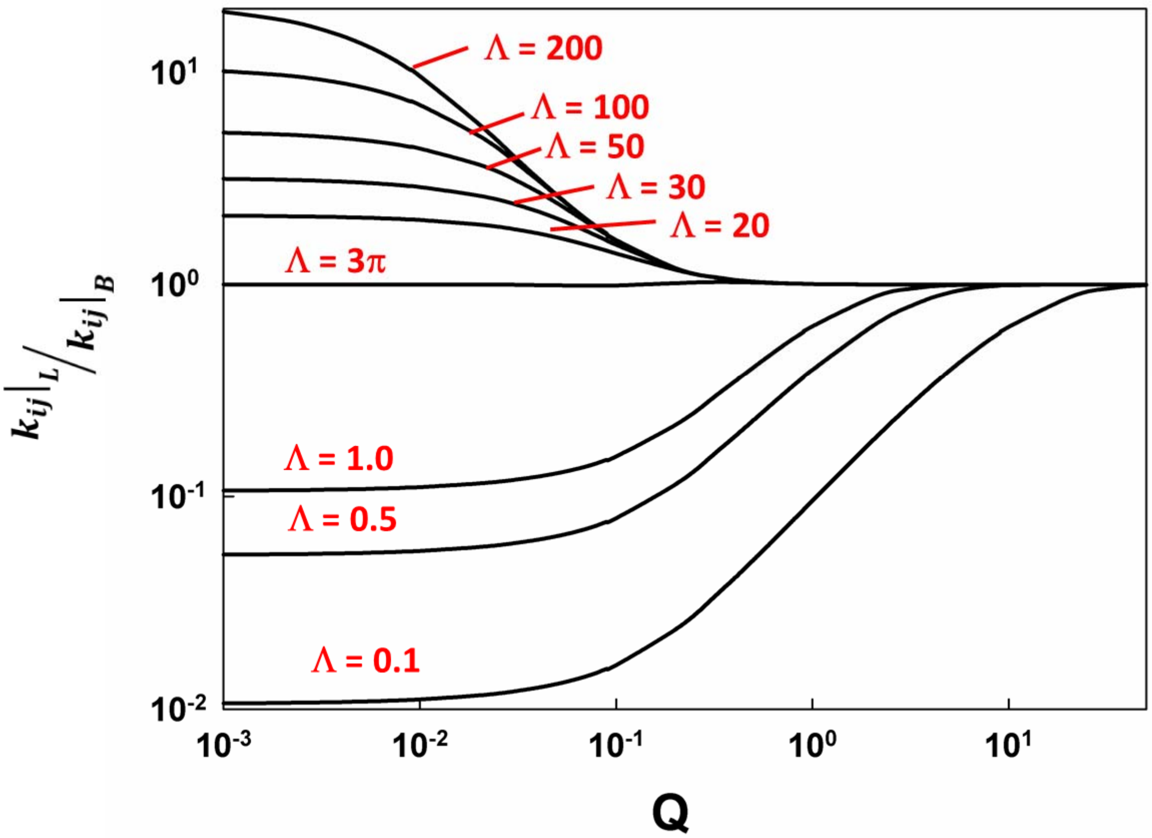

Figure 7. The ratio of the laminar shear collision rate coefficient to the Brownian motion collision rate coefficient for oppositely charged particles, considering the Coulomb potential with St = 0.